Clinical Cancer Research

ATR Inhibition Potentiates the Radiation-induced Inflammatory Tumor Microenvironment

Magnus T. Dillon, Katharina F. Bergerhoff, Malin Pedersen, Harriet Whittock, Eva Crespo-Rodriguez, Emmanuel C. Patin, Alex Pearson, Henry G. Smith, James T.E. Paget, Radhika R. Patel, Shane Foo, Galabina Bozhanova, Chanthirika Ragulan, Elisa Fontana, Krisha Desai, Anna C. Wilkins, Anguraj Sadanandam, Alan Melcher, Martin McLaughlin, and Kevin J. Harrington

Abstract

Purpose: ATR inhibitors (ATRi) are in early phase clinical trials and have been shown to sensitize to chemotherapy and radiotherapy preclinically. Limited data have been published about the effect of these drugs on the tumor microenvironment.

Experimental Design: We used an immunocompetent mouse model of HPV-driven malignancies to investigate the ATR inhibitor AZD6738 in combination with fractionated radiation (RT). Gene expression analysis and flow cytometry were performed posttherapy.

Results: Significant radiosensitization to RT by ATRi was observed alongside a marked increase in immune cell infiltration. We identified increased numbers of $CD3^+$ and NK cells, but most of this infiltrate was composed of myeloid cells. ATRi plus radiation produced a gene expression signature matching a type I/II IFN response, with upregulation of genes playing a role in nucleic acid sensing. Increased MHC I levels were observed on tumor cells, with transcript-level data indicating increased antigen processing and presentation within the tumor. Significant modulation of cytokine gene expression (particularly CCL2, CCL5, and CXCL10) was found *in vivo*, with *in vitro* data indicating CCL3, CCL5, and CXCL10 are produced from tumor cells after ATRi + RT.

Conclusions: We show that DNA damage by ATRi and RT leads to an IFN response through activation of nucleic acid–sensing pathways. This triggers increased antigen presentation and innate immune cell infiltration. Further understanding of the effect of this combination on the immune response may allow modulation of these effects to maximize tumor control through antitumor immunity.

Introduction

In recent years, we have begun to understand that the effects of anticancer therapies cannot be considered purely from the narrow perspective of their ability to kill cancer cells effectively. Instead, their effects on the tumor microenvironment are increasingly recognized as playing a major role in the success or failure of treatment. An appreciation of the importance of the immune system to cancer surveillance, development, and response to treatment has highlighted the effect that radiation has on the microenvironment, and has served as a driver of research into combinations of radiation and immune-targeted therapies (1). At the same time, increasing recognition of the effect of the vasculature and stroma on tumor control and normal tissue side-effects of radiotherapy has highlighted potential new targets for intervention (2).

Radiation has positive and negative effects on the tumor microenvironment. Radiation increases antigen presentation and T-cell priming, and can stimulate systemic (abscopal) antitumor responses, particularly when coadministered with immune checkpoint blockade (3). On the other hand, it can stimulate suppressive cells such as myeloid-derived suppressor cells (MDSC) and tumor-associated macrophages (TAM), which have been associated with tumor angiogenesis and invasion (4). Links between the DNA damage response (DDR) and both autoimmunity and anticancer immunity are increasingly being described. The stimulator of interferon genes (STING) pathway, activated by cytosolic DNA, stimulates type I IFN production, leading to immune responses (5). Defective DDR, S-phase DNA damage, and micronucleus formation can trigger IFN production and alter the expression/function of cell surface immunomodulatory molecules (6–8). Targeted anticancer therapies can also exert diverse effects on the immune microenvironment (9). Few data have been reported on the microenvironmental effects of radiation in combination with radiosensitizing agents, such as DDR inhibitors. Understanding these effects may provide opportunities for further therapeutic benefit, especially in terms of immunotherapy strategies.

Here, we show that the ATR inhibitor, AZD6738, alone and in combination with a clinically relevant fractionation schedule of radiotherapy modulates the immune tumor microenvironment. To our knowledge, this is the first comprehensive profiling of the immune tumor microenvironment in the context of targeted radiosensitization.

The Institute of Cancer Research, London, United Kingdom.

Note: Supplementary data for this article are available at Clinical Cancer Research Online (http://clincancerres.aacrjournals.org/).

M. McLaughlin and K.J. Harrington are the co-senior authors of this article.

Corresponding Author: Magnus T. Dillon, Institute of Cancer Research, Chester Beatty Laboratories, 237 Fulham Road, London SW3 6JB, United Kingdom. Phone: 44-20-7153-5150; E-mail: magnus.dillon@icr.ac.uk

Clin Cancer Res 2019;25:3392–403

doi: 10.1158/1078-0432.CCR-18-1821

Translational Relevance

AZD6738 is currently under investigation in clinical trials in combination with radiotherapy (NCT02223923). Substantial preclinical data exist on the radiation-potentiating effects of drugs inhibiting components of the DNA damage response. Given the increased understanding of the pivotal role of the immune system in cancer control, it is critical to understand the effect radiosensitizer compounds have on the tumor microenvironment, specifically their impact on the immune system and its responses. AZD6738 boosts the immunogenic effect of radiation, enhancing tumor-derived cytokine production, antigen presentation, and infiltration of myeloid lineage immune populations. Both inflammatory and immunosuppressive cells are increased after the combination treatment. The modulation of these responses to maximize antitumor immunity and effect on adaptive responses will be the subject of future study.

Materials and Methods

Animals and cell lines

All experiments were approved by the Institutional Review Board and complied with National Cancer Research Institute guidelines (10). TC-1 cells, a modified mouse lung epithelial cell line transformed with HPV-16 E6 and E7 and oncogenic HRAS, were a kind gift from Prof. Tzyy-Choou Wu (Johns Hopkins University, Baltimore, MD; ref. 11) and Prof. Eric Deutsch (Institut Gustave Roussy, Villejuif, France). Two million cells were injected subcutaneously into the right flank of female C57Bl/6 mice; treatments were started 7–8 days later, at which point tumors were 50–100 mm^3. The experimental endpoint for growth delay experiments was a tumor diameter of 15 mm or greater.

Drugs

AZD6738 was provided by AstraZeneca and was dissolved in 10% DMSO, 40% propylene glycol, 50% water, and administered by oral gavage, 2 hours before irradiation. For hypoxia studies, pimonidazole (Hypoxyprobe, HPI) 60 mg/kg was injected intraperitoneally 1 hour prior to tissue collection.

Irradiation

Animals were irradiated under anesthesia with Hypnorm (Fentanyl/fluanisone, Vetapharma) and Midazolam (Roche) given intraperitoneally. Irradiation was performed using an AGO 250 kV X-ray machine at a dose rate of 1.62 Gy/minute (AGO). Animals were irradiated in the prone position positioned under lead shielding with a 16-mm diameter aperture aligned over the tumor. Radiation dose was measured using a Farmer Chamber and Unidos-E Dosemeter (both PTW).

Immunophenotyping

Viability dye: eBioscience fixable viability dye eFluor 780 (65-0865-14). Antibodies: conjugated antibodies were obtained from BioLegend unless otherwise stated. Antibodies used are shown in Supplementary Table S1. Tumors were harvested and kept on ice, then blotted dry, and weighed before mechanical dissociation with scissors and enzymatic digestion for 30 minutes at 37°C with (per sample) 40 μL 0.25% trypsin, 20 μL collagenase (Sigma C1639 25 mg/mL in PBS), 2 μL dispase (200 mg/mL), and 10 μL DNAse (20 mg/mL), before passing through a 70-μm cell strainer and rinsing with RPMI supplemented with 10% FCS and 5 mmol/L EDTA. Samples were resuspended in PBS with 5% FCS, blocked with anti-CD16/32 antibody (BioLegend 101319) for 10 minutes on ice, and then stained immediately on ice in a staining volume of 40 μL, diluting antibodies at the dilutions given in Supplementary Table S1 in PBS with 5% FCS for 30 minutes before washing twice. For intracellular epitopes, samples were fixed and permeabilized after staining for extracellular epitopes, using the FoxP3/Transcription factor Fixation/Permeabilization Kit (eBioscience 00-5521-00, Thermo Fisher Scientific) in accordance with the manufacturer's protocol. Subsequent staining was performed using the permeabilization buffer from this kit. After fixation, samples were washed twice and fixed using 1% formaldehyde in PBS before acquisition on a BD LSRII Flow Cytometer (BD Biosciences). Photomultiplier tube voltages were set using fully stained samples, and compensation was performed using single-stained UltraComp eBeads (eBioscience). Gating was performed using "fluorescence minus one" controls and a limited number of isotype controls were used (Supplementary Table S1). The sample was divided equally into staining panels and each sample was acquired entirely. Data were analyzed using FlowJo software (FlowJo); counts were normalized to tumor weight and corrected for the number of panels into which the sample was divided.

RNA analysis

Tumor samples were harvested from animals and stored in RNALater (AM7020, Thermo Fisher Scientific) at −20°C prior to RNA extraction. Samples were processed by homogenization using a Precellys24 Homogenizer (Bertin Technologies) and RNA extraction performed using RNEasy Kit (74104, Qiagen) as per the manufacturer's protocol. Paired $CD45^-$ and $CD45^+$ samples were generated by disaggregation and staining using CD45 30-F11 as for immunophenotyping. Sorting was performed using a FACS Aria III. Samples were kept on ice at all times other than enzymatic digestion; sort was performed under chilled conditions. RNA extraction on sorted cell pellets was by RNEasy Kit. Extracted RNA was quantified using a NanoDrop Spectrophotometer (Thermo Fisher Scientific) and quality assessed on a BioAnalyzer 2100 (Agilent). Samples were stored at −80°C before further analysis. One-hundred nanograms of RNA was used for the analysis using the nCounter PanCancer Immune Profiling Panel (XT-CSO-MIP1-12, NanoString Technologies). Data analysis was performed using the nSolver Advanced Analysis Software (NanoString Technologies). PTPRC (CD45) transcript counts in sorted samples postnormalization ranged from 20 to 129 in $CD45^-$ and 9234 to 11298 for $CD45^+$ samples. As a precaution, minor $CD45^+$ contamination of treated $CD45^-$ (0.9%–0.3%) was corrected for by subtraction of the corresponding percentage of transcripts from paired $CD45^+$ samples calculated on the basis of PTPRC transcript counts. This was to avoid false-positive changes associated with isolated high transcript genes. Differential expression was compared between two conditions, *P* values were adjusted using the Benjamini–Yekutieli FDR; genes with $P_{adj} < 0.05$ are displayed. Functional annotations were based on gene ontology terms.

IHC

IHC was performed at the Breast Cancer Now core histopathology facility, using the following primary antibodies. Dako

Flex Envision (K8002) was used as the secondary reagent: p^{S345}Chk1, Thermo Fisher Scientific PA5-34625; CD3, Dianova clone SZ31, DIA-310; CD45R, Abcam ab64100; Pimonidazole, hypoxyprobe, MAb1; Carbonic Anhydrase IX: Abcam ab15086; Smooth muscle actin, Dako clone 1A4, M0851.

Western blot analysis

Snap-frozen tumor samples were lysed in RIPA buffer using a Precellys 24 Homogenizer (Bertin Technologies). All lysates were quantified by BCA Assay (Thermo Fisher Scientific) prior to SDS-PAGE and Western blotting. The following antibodies were used: GAPDH 14C10, MDA5 D74E4, and cGAS D3O8O (Cell Signaling Technology). Secondary was IRDye 800CW Goat anti-Rabbit IgG H + L and imaged using a LI-COR Odyssey CLx (LI-COR Biosciences).

Statistical analyses

Statistical analysis was performed using Prism 7 (GraphPad Software). For tumor growth delay, means of radiation and radiation + ATRi groups were compared using Student unpaired *t* test. Flow cytometry cell counts, mRNA count and proportions, and fluorescence data were compared using one-way ANOVA with Tukey multiple comparisons test. An asterisk indicates $P \leq 0.05$. Where multiple asterisks are used, ** indicates $P \leq 0.01$, *** indicates $P \leq 0.001$, and **** indicates $P \leq 0.0001$.

Results

ATRi and ATRi-RT modulate the immune microenvironment

Two participants in the dose-escalation study of AZD6738 monotherapy (12) had tumor volume reductions. We noted that this was associated with an inflammatory infiltrate in one of the participants, and hypothesized that AZD6738 may have a modulating effect on the immune tumor microenvironment. We sought to investigate how AZD6738 may modulate radiation-induced changes to the tumor microenvironment (TME).

TC-1 is an immunocompetent model of HPV-driven malignancies. This model was chosen as it has previously been used for examining immune responses to radiotherapy combinations, and it was moderately sensitive to combination therapy, allowing sufficient tumor for analysis at the time point chosen. Mice bearing subcutaneous TC-1 tumors were treated 8 days after implantation, at which point tumors were 50–100 mm^3. Mice were dosed with vehicle or AZD6738 (75 mg/kg daily), starting 2 hours before the first dose of radiation, with the last dose given on day 5. Irradiation was given daily, 2 hours after drug or vehicle dosing, at 2 Gy per fraction for 4 days. ATR inhibition sensitized this model to radiation, with significantly greater tumor growth delay (Fig. 1A) and a significant increase in survival to humane endpoint (Supplementary Fig. S1A).

Initial profiling of the TME was carried out 5 days after irradiation on formalin-fixed tissue. This was focused on broad markers investigating vessel density, hypoxia, fibroblasts, $CD3^+$ (T), and $CD45R/B220^+$ (B) cells. Because hypoxia is an important determinant of radiosensitivity, we wanted to examine whether the radiosensitization by AZD6738 was due to modulation of perfusion or hypoxia. Microenvironmental markers of hypoxia (pimonidazole, CAIX) and fibroblasts (αSMA) did not differ significantly between treatment groups (Supplementary Fig. S2A–S2C). Vessel density after 4 × 2 Gy measured by CD31 had significantly reduced compared with control. When AZD6738 was added to radiation this reduction was reversed (Supplementary Fig. S2D). We did observe increased numbers of T cells (Fig. 1B) and B cells (Fig. 1C) after combination treatment with radiation and AZD6738. Given these findings, further work focused in detail on the effect of ATRi plus radiation (ATRi-RT) on the immune tumor microenvironment.

ATRi-RT modulates multiple immune-related genes

NanoString-based expression profiling of TC-1 tumors was carried out to comprehensively profile gene expression changes 5 days after the end of radiation. This time point was selected initially to focus more on infiltrating immune population markers post-DNA damage. This revealed changes in expression in multiple categories of genes due to radiation or AZD6738 alone, with the addition of AZD6738 potentiating radiation-induced changes (Fig. 2A). This was particularly pronounced in the gene ontology groups CD molecules, apoptosis, adaptive antigen processing, and MHC. Numbers of genes with significant differential expression are shown in Fig. 2B. Strikingly, we found evidence of an IFN response, with large changes in expression of a number of IFN-stimulated genes (Fig. 2C; ref. 13; Supplementary Figs. S3 and S4). Numerically, the combination of ATRi and radiation caused the largest number of changes and greatest degree of change in gene expression.

These gene expression changes suggest infiltration and activation of innate and adaptive immune cells, which was maximal after combined ATRi-RT treatment.

ATRi-RT increases lymphocyte infiltration

Flow cytometry was used to validate specific intratumoral cell population data identified by gene expression analysis presented in Fig. 2. A more focused analysis was also undertaken in the draining lymph nodes. The general lymphoid gating strategy for FACS analysis is shown in Supplementary Figs. S5 and S6.

Greater numbers of total $CD3^+$ cells over control were demonstrated after treatment with ATRi, radiation, and maximal levels were seen with combination therapy (Fig. 3A, this observation was maintained when analyzed for the total number of cells; Supplementary Fig. S7). There were also significantly increased numbers of $CD4^+$ $FOXP3^+$ T_{regs} and NK cells. There was a nonsignificant trend toward increase in $CD8^+$ cells observed with combination therapy (Fig. 3A), with a higher proportion of $CD8^+$ granzyme B^+ as well as $CD8^+$ $Ki67^+$ cells observed with combination therapy (Fig. 3B). This correlated with transcript-level data observed, where *Cd8a*, granzyme B (*Gzmb*), and perforin (*Prf1*) were highest in the combination group (Fig. 3C).

Analysis of markers of activation and proliferation showed a significantly increased proportion of proliferating T_{regs} with the combination treatment (Fig. 3B). These results confirmed the transcriptional analysis, which showed increased T-cell–associated and *Foxp3* transcripts in tumors (Fig. 3C). The draining lymph nodes also contained an increased proportion of proliferating $Ki67^+$ T_{regs} as a function of total T_{regs} (Fig. 3D).

To further define infiltrating lymphocytes, flow cytometry was performed on T-cell subsets with a selection of markers (Fig. 3E). Although not statistically significant, a consistent trend was observed for increased expression of LAG3, TIM3, ICOS, and CTLA4 on $CD4^+$ effector cells in the ATRi-RT combination group. No significant changes in fluorescence were found in T_{regs} or $CD8^+$ T cells (data not shown). Similar but more statistically significant changes were observed at the transcript level. *Havcr2* (TIM3), *Tigit*,

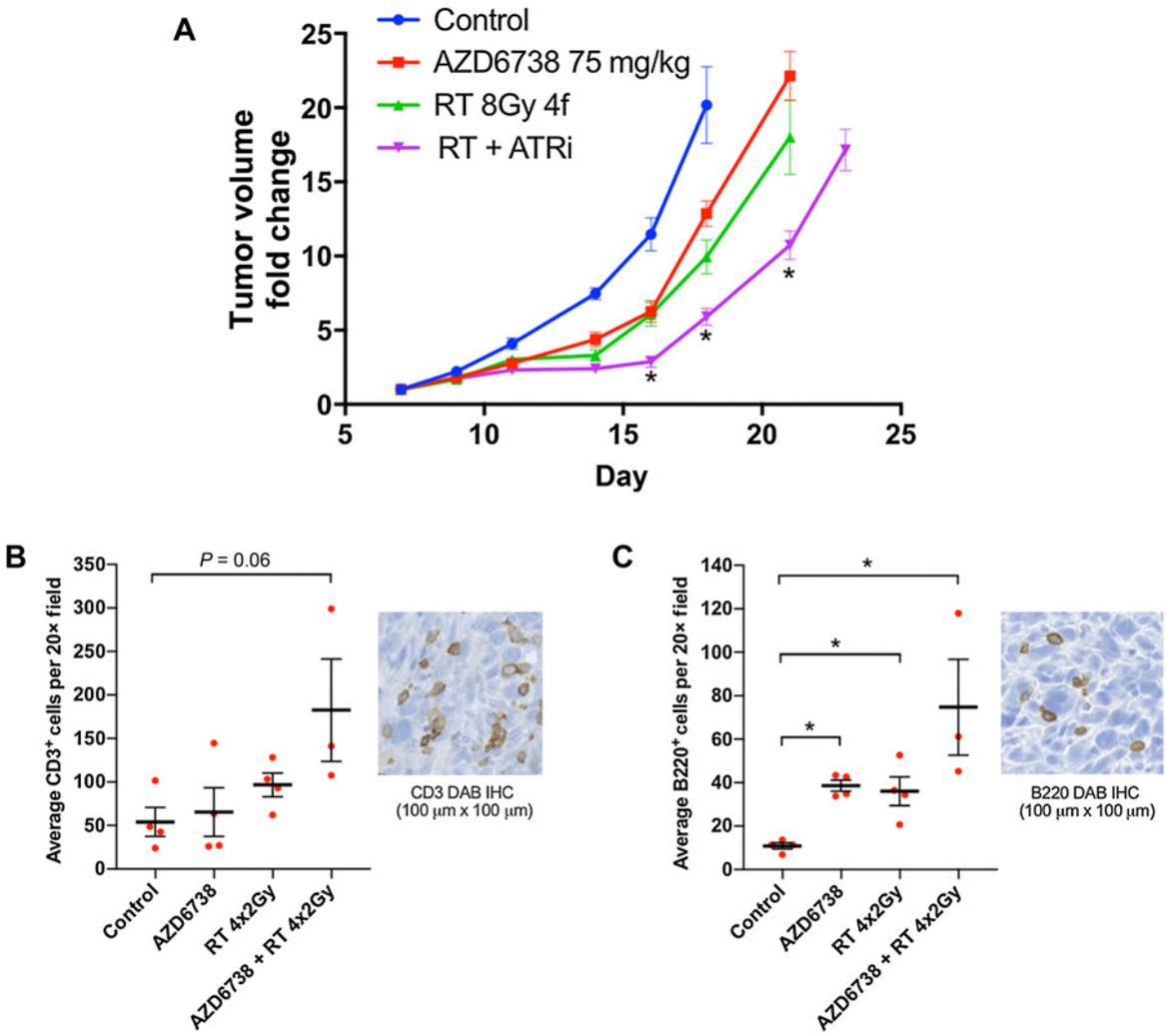

Figure 1.

AZD678 therapeutic efficacy combined with fractionated radiotherapy *in vivo* corresponds to increased $CD3^+$ and $B220^+$ cell infiltration by IHC. **A,** Relative tumor growth curves for C57Bl/6 mice carrying subcutaneous TC1 tumors, treated with vehicle, AZD6738 75 mg/kg daily for 5 days, radiation 2 Gy x 4 (daily fractions), or AZD6738 with radiation; the first dose of AZD6738 was administered 2 hours prior to irradiation, and the last dose was administered the day after the final fraction of radiation. Asterisk represents $P < 0.05$ between radiation and radiation + ATRi curves by unpaired *t* test. Minimum 10 animals per group. **B,** Quantification of TC1 tumors from (**A**) stained for CD3 by IHC. Minimum 10 fields of view and at least 3 tumors analyzed per condition. Average number per field is shown for each tumor; tumors were harvested 5 days after the last fraction of radiation was administered. **C,** Quantification of $B220^+$ cells, as per (**B**).

Icos, and *Eomes* were upregulated in ATRi-RT compared with control or either monotherapy (Supplementary Fig. S8A). Further mRNA analysis showed increased numbers of transcripts associated with a Th1 response, including *Il12rb2*, *Ctla4*, and *Stat4* (Supplementary Fig. S8B) between control and RT, control, and ATRi-RT. When transcriptional analysis was performed on sorted $CD45^+$ tumor-infiltrating cells alone, there was a significant increase in *Gzmb* transcripts (Fig. 3F). Taken together, these data suggest increased T_{reg} proliferation as well as evidence of CD4 effector cell activation or exhaustion with combination treatment.

ATRi-RT causes an increase in myeloid cell infiltration

Further validation of gene expression data identified that AZD6738 and radiation induced substantial infiltration of myeloid innate immune cells (Fig. 4A; Supplementary Fig. S7B). The general myeloid-gating strategy for FACS analysis is shown in Supplementary Fig. S6. A significant increase was seen in tumor-infiltrating dendritic cells (DC), macrophages (Mac), and a $CD11b^+Gr1^+$ population (Fig. 4A; ref. 14). This increase was clear but not statistically significant compared with controls for both monotherapies, but highest and statistically significant for ATRi in combination with radiation. In absolute numbers, the cumulative infiltration of these three populations was approximately three times the total number of $CD3^+$ cells in the combination group (Figs. 3A and4A).

Flow cytometry was used to determine whether ATRi-RT altered specific subpopulations of DCs, Macs, or $CD11b^+Gr1^+$ cells. On the basis of CD206 staining, we did not detect any change in the proportions of M2-like Macs (Fig. 4B). Ly6C, a monocytic marker, showed that there was no clear shift in the monocytic

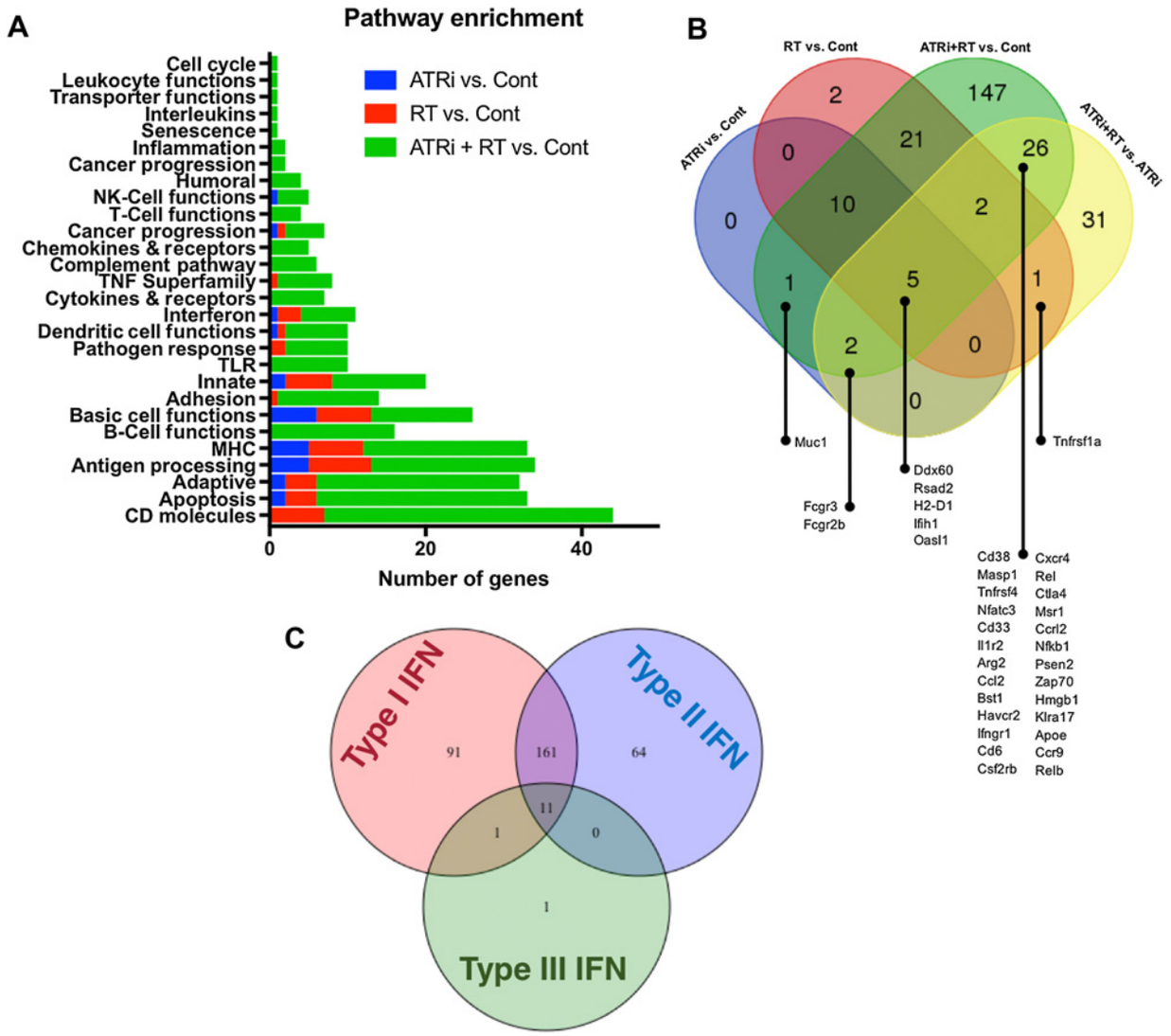

Figure 2.

Gene expression analysis reveals AZD6738 significantly modulates radiation-induced immune-linked transcripts *in vivo*. **A,** Overview of differential gene expression with ATR-radiation combinations in the TC-1 murine model at 5 days after the end of 4 × 2 Gy radiation in the presence or absence of AZD6738. Differential expression analysis of NanoString data was performed, and gene functional annotations used to classify each gene with significantly altered expression into one of the above groups. Genes with significant change in expression (with $P < 0.05$ by Benjamini–Yekutieli Method) were grouped into functional categories, and the number of genes with significant differential expression per category is shown for the indicated pairwise comparisons. Legend indicates which two groups were compared. **B,** Venn diagram illustrating numbers of genes with significant changes in expression for the indicated combinations. **C,** Venn diagram illustrating ISGs, for ATRi-RT combination treatment. The number of genes stimulated by each of type I, II, and III IFNs is demonstrated. Overall, there is a greater representation of genes that are stimulated by type I IFNs in the database, and very few by type III IFNs, so this may lead to a degree of bias in these results (from Interferome database).

$CD11b^+Gr1^+$ cell population with combination treatment versus control (Fig. 4C). On the other hand, granulocytic marker Ly6G staining showed that the numbers of granulocytic $CD11b^+Gr1^+$ cells were lower (Supplementary Fig. S6). Two subsets of DCs, classical (cDC) and plasmacytoid (pDC), were investigated because pDCs have Toll-like receptors 7 and 9, which sense RNA and DNA, respectively. We hypothesized that the increased DNA damage with ATR inhibition may activate these pattern recognition receptors. Tumor-associated pDCs may increase tumor–antigen presentation or may be tolerogenic (15). B220 has been described as a marker for pDCs in $CD11c^+$ DC (15). No difference was found in proportions of pDCs and cDCs, using flow cytometric analysis of CD11c and B220 staining, with cDCs making up the majority of DCs within the tumor, and numbers of both increasing with ATRi-RT treatment (Fig. 4D). Although ATRi-RT increases both the numbers of DCs and TAMs, it does not alter the DC subsets investigated, or the polarity of TAMs.

We noted an increase in both PD-1 and PD-L1 mRNA with ATRi and ATRi-RT therapy (Supplementary Fig. S8C), which confirmed

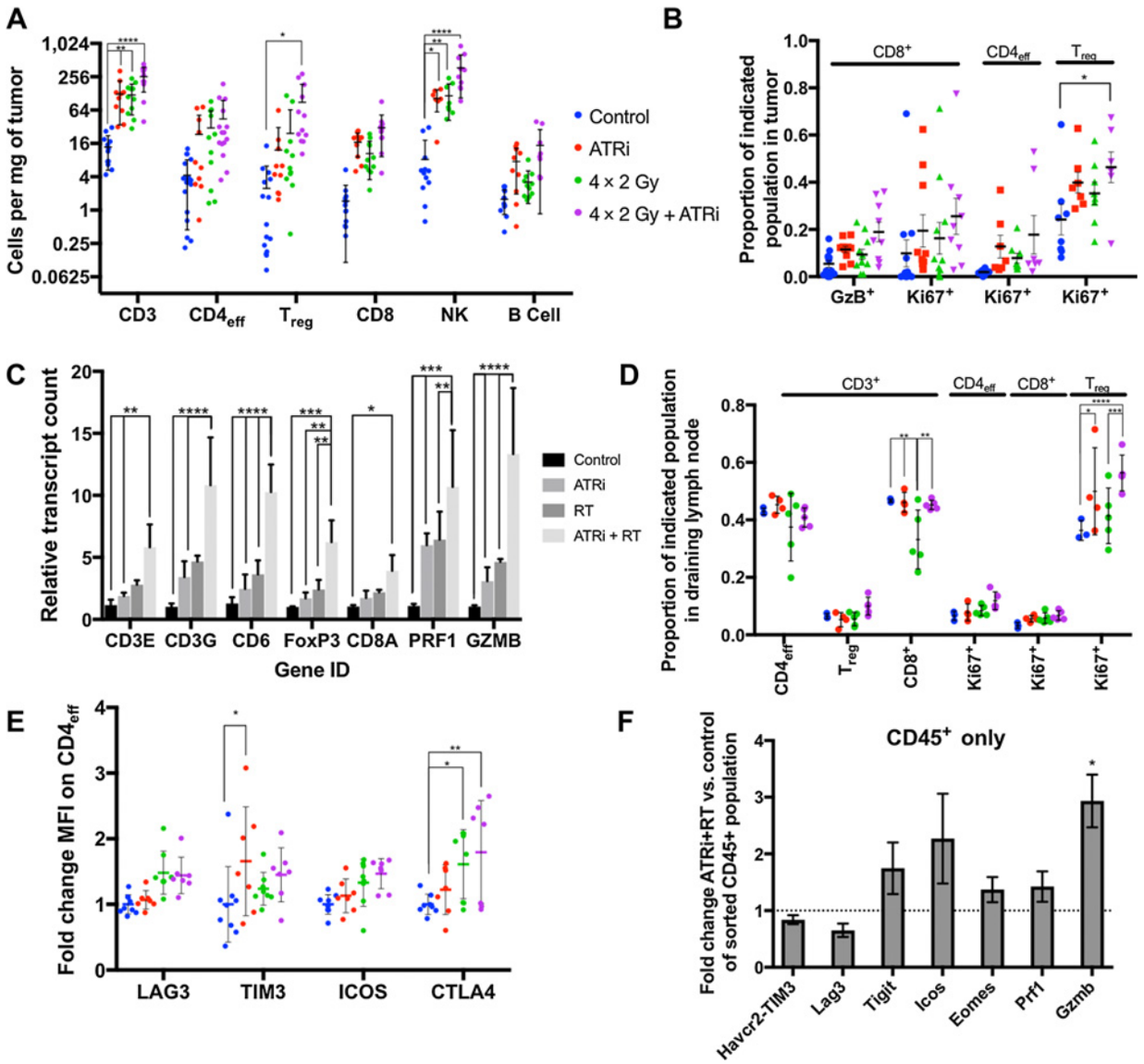

Figure 3.

AZD6738 increases radiation-induced lymphoid infiltration *in vivo*. **A,** Number of lymphoid cells per mg tumor was calculated 5 days after the end of 4 × 2 Gy radiation in the presence or absence of AZD6738. Error bars, SD (one direction only if lower SD outside the plotted area); asterisks, statistical significance by ANOVA with multiple comparisons, minimum 3 independent repeats of at least 3 animals per group. Populations were identified by the markers: CD3, $CD3^+$; CD4eff, $CD3^+CD4^+FOXP3-$; T_{reg}, $CD3^+CD4^+FOXP3^+$; CD8, $CD3^+CD8^+$; NK, $CD3^-B220^-NK1.1^+$; B cell, $B220^+$. **B,** Change in proportion of Granzyme B (GzB^+) or $Ki67^+$ $CD8^+$ cells as a proportion of total $CD8^+$ cells, and $Ki67^+$ (proliferating) cells as a proportion of total $CD4^+FOXP3^-$ or $CD4^+FOXP3^+$ cells. Error bars, SEM. **C,** mRNA transcript fold change in whole-tumor lysates at 5 days after completion of radiotherapy. Copy number normalized to median controls. Mean and SD plotted, asterisks, statistical significance by ANOVA with multiple comparisons. **D,** Change in proportion of effector, regulatory, and $CD8^+$ T cells, as a function of total $CD3^+$ cells, and $Ki67^+$ T_{reg}, $T_{eff,}$ and $CD8^+$, as a proportion of total T_{reg}, $T_{eff,}$ and $CD8^+$ cells, in draining lymph node (ipsilateral inguinal node), 5 days after completion of radiotherapy, minimum 3 animals per group. **E,** Normalized fluorescence intensity (normalized to mean of control fluorescence) of effector CD4 T cells ($CD3^+$, $CD4^+$, $FoxP3^-$), for the indicated markers of activation in tumor-infiltrating cells in TC-1 tumors 5 days after the end of 4 × 2 Gy radiation in the presence or absence of AZD6738. Minimum 3 animals per group in 2 independent experiments. **F,** Fold change mRNA transcript counts for corresponding genes indicating T-cell activation, in a cell population sorted for CD45 in ATRi-RT–treated tumors, relative to the median value for the control samples of each gene, mean and SD are plotted. Asterisks, significance by unpaired *t* test between ATRi-RT and control.

flow cytometry analysis, finding that the predominant increase in PD-L1 signal was from $CD45^+$ CD3− cells, with a relatively minor contribution from tumor cells (Fig. 4E). Transcriptional analysis of sorted tumor-infiltrating immune cells and $CD45^-$ cells, a surrogate for tumor cells, showed a significant increase in *Cd274* (PD-L1) transcripts in both populations (Fig. 4F). Previous data have shown that tumor-infiltrating MDSC and Macs are PD-$L1^+$ (16, 17), and our observations have confirmed this, with increasing PD-L1 positivity after treatment with ATRi, radiation, and the combination (Fig. 4E).

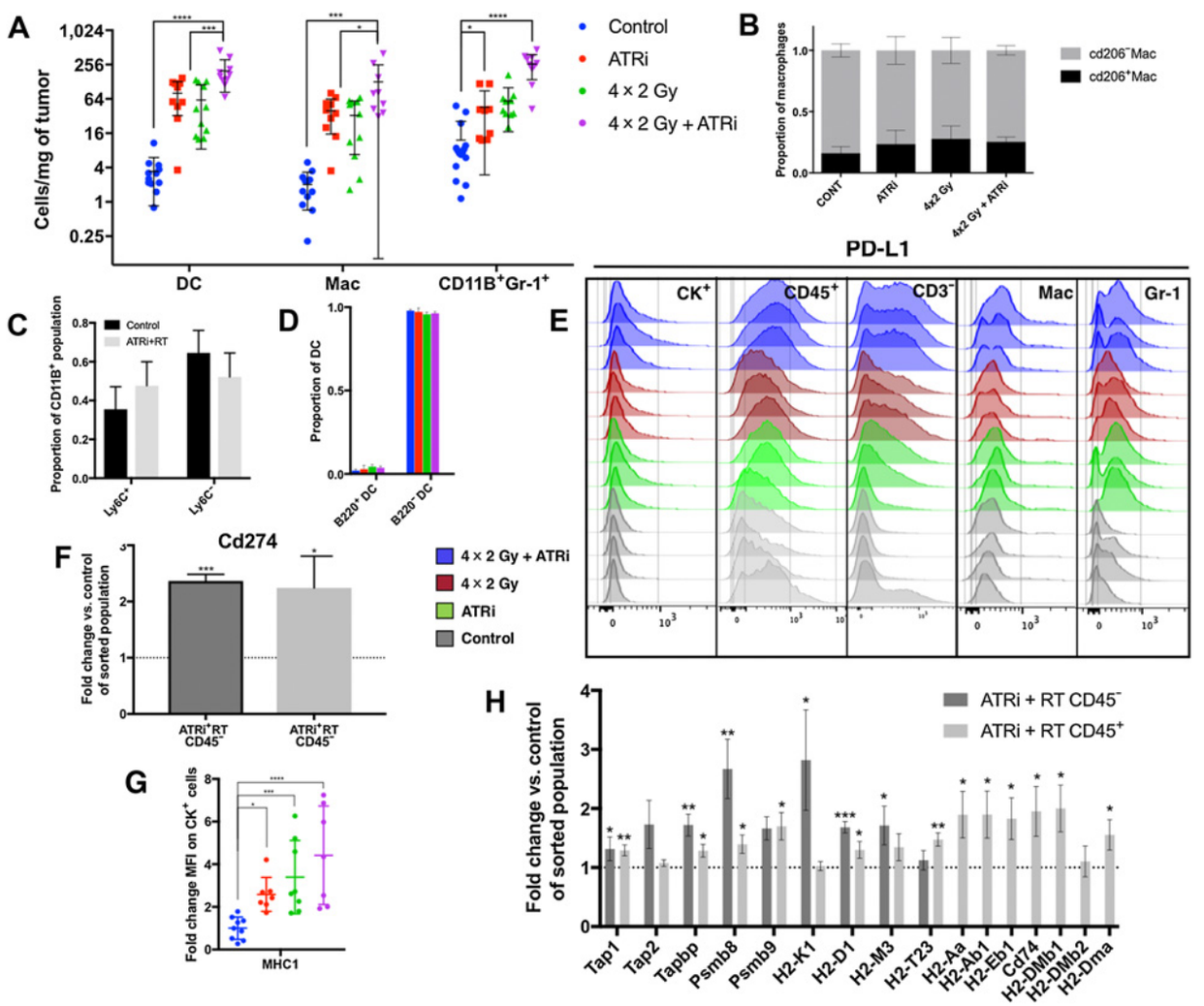

Figure 4.

AZD6738 increases radiation-induced myeloid infiltration *in vivo*. **A,** Assessment of tumor-infiltrating myeloid cells at day 5 after treatment. Populations were identified as follows: B cells, $B220^+$; DCs, $CD11c^+$ $MHCII^+$; Macs, $CD11b^+$ $CD11c^-$ $CD68^+$ SSC^{Low}, MHC-2^+, Gr-$1^{Low\text{-}Int}$; $CD11b^+$ $Gr1^+$, $CD11b^+$ Gr-$1^{Int\text{-}Hi}$ $NK1.1^-$ $CD3^-$. Asterisks, statistical significance by ANOVA with multiple comparisons testing. **B,** Proportions of $CD206^+$ and $CD206^-$ tumor-infiltrating Macs, as a marker of M2a and M2c Macs. **C,** Proportions of $CD11b^+Gr\text{-}1^+$ subsets: proportions of $CD11b^+$ $Ly6C^{High}$ for monocytic and $Ly6C^{Low}$ for granulocytic, no significant difference between control and ATRi+RT. **D,** Dendritic cells ($CD11C^+$ $MHC2^+$) were stained with B220, a marker of pDC. Proportion of parent shown. **E,** Flow cytometric analysis of PD-L1 staining for the indicated tumor subpopulations: CK^+ indicates pan-cytokeratin–positive cells, a surrogate for tumor cells. Mac, Macrophages ($CD11b^+$, CD3–, $NK1.1^-$, $CD11c^{Low}$, $CD68^+$, $MHCII^+$, Gr-$1^{Low\text{-}int}$); Gr-1, $CD11b^+$, Gr-1^+, $CD3^-$ $NK1.1^-$ **F,** mRNA counts for PD-L1 (*Cd274*), expressed as fold change in ATRi-RT–treated tumors compared with control, in tumor populations sorted by CD45 status. **G,** Flow cytometric analysis of tumor cells (pan-cytokeratin–positive), showing mean fluorescence intensity for MHC-1 (mouse: H-2Kb). Mean fluorescence normalized to average control value. **H,** mRNA expression of genes involved in antigen processing and presentation, fold change in ATRi-RT versus control, expressed as fold change in ATRi-RT–treated tumors compared with control, in tumor populations sorted by CD45 status. All panels, 5 days after the end of treatment with 4 × 2 Gy radiation in the presence or absence of AZD6738. Minimum 3 tumors per condition, 2 independent experiments. Significance, ANOVA with multiple comparisons (except F, H: unpaired *t* test), mean, and SD displayed.

Using pan-cytokeratin as a marker for tumor cells, we observed a significant increase in MHC-I expression, with all conditions compared with control (Fig. 4F). Pan-cytokeratin is generally expressed on tumor cells, but may not be specific to these. mRNA expression data confirmed the increase in H2 complex molecules on $CD45^-$ cells, as well as a number of other components involved in antigen processing and presentation on both $CD45^+$ and $CD45^-$ cells. These include H2 class I on tumor cells, class II on immune cells, and other genes involved in the antigen presentation processes (Fig. 4H).

ATRi and radiation drive immune cell infiltration through tumor cell–intrinsic cytokine release

ATRi and radiation clearly drive immune cell infiltration, particularly of the myeloid compartment, in response to therapy. The process driving this infiltration was, however, not clear. To investigate the potential trigger for immune cell infiltrates seen after ATRi-RT, differential expression for cytokine and cytokine receptor mRNAs was analyzed (Fig. 5A). In all cases statistically significant changes were observed at the transcript level for ATRi-RT. The greatest changes after the combination of ATRi-RT were in

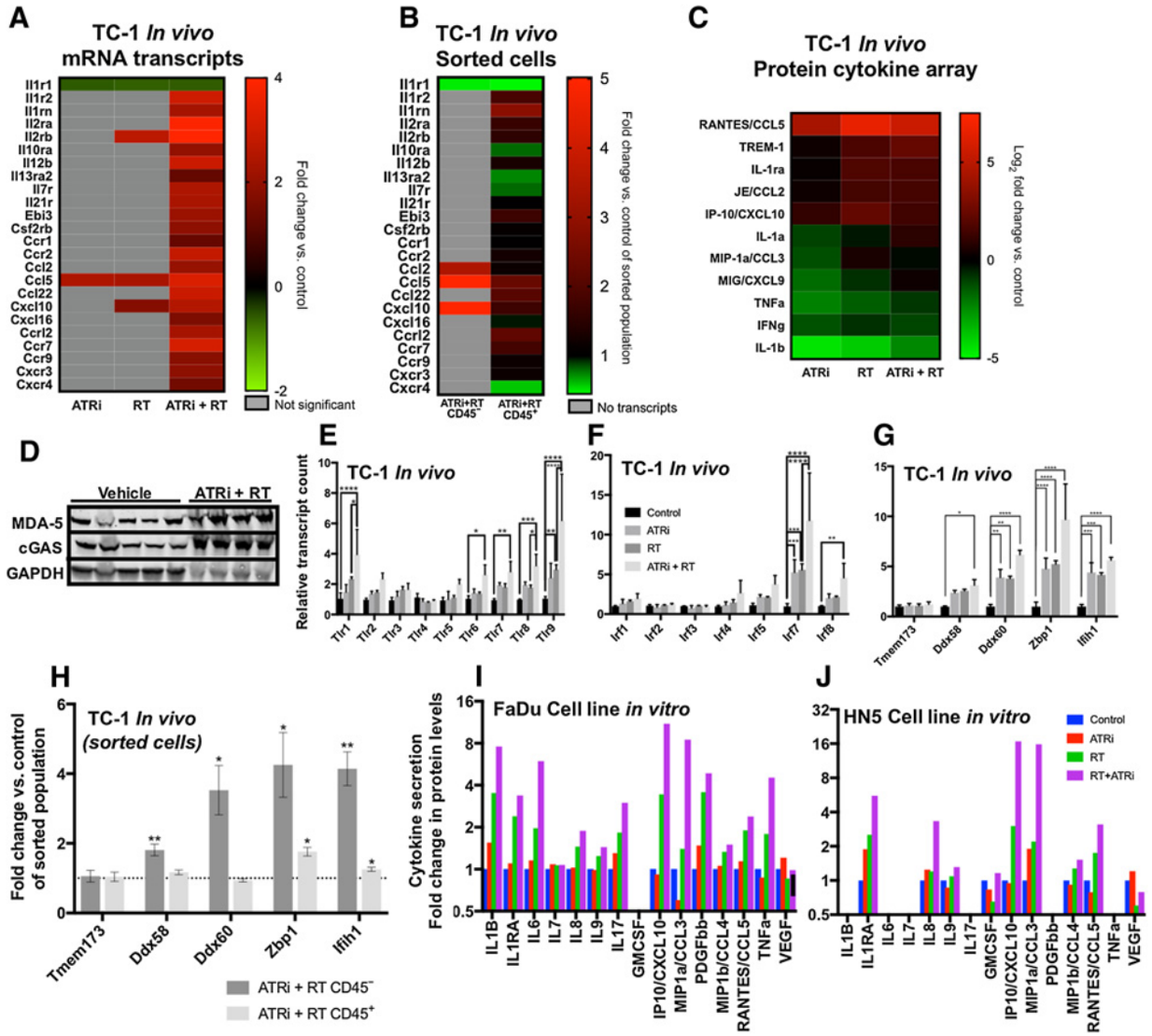

Figure 5.

ATRi-RT causes modulation of cytokine production. Analysis of changes in cytokine expression with ATR–radiation combinations, 5 days after treatment with 4 × 2 Gy radiation in the presence or absence of AZD6738. **A,** mRNA expression data; only statistically significant changes are displayed. Mean of 3 replicates displayed. Fold change from control tumors displayed. Gray boxes, no significant difference found. **B,** Cytokine, chemokine, and receptor transcript analysis, as for **A,** in tumor populations sorted by CD45-status. Gray boxes, no transcripts. **C,** Protein expression by cytokine array. Densitometry of array was measured and then normalized to positive and negative controls. Two tumors per group were analyzed in duplicate. Mean of 2, $\log_2$ fold change replicates displayed. **D,** Western blot showing changes in the indicated proteins in *in vivo* samples after vehicle or ATRi+RT treatment, 5 days after the end of irradiation. **E,** mRNA expression of Toll-like receptor (TLR) transcripts. **F,** mRNA expression of IFN regulatory factor (IRF) transcripts. **G,** mRNA expression of the indicated nucleic acid–sensing proteins. **A–G,** At 5 days after the final dose of radiotherapy, 3 animals per group, mean and SD displayed, analyzed by ANOVA with multiple comparisons. **H,** Analysis of transcripts for nucleic acid sensors as for **G**, on sorted populations of $CD45^+$ and $CD45^-$ tumor cells. Asterisk, Significance by unpaired *t* test compared with control group for same cell population. **I** and **J,** Measurement of cytokine concentration in supernatant of tumor cell lines FaDu (**I**) and HN5 (**J**) at 72 hours after treatment with DMSO, AZD6738 (0.5 μmol/L), an 8 Gy fraction of radiation, or radiation in combination with AZD6738 (added 1 hour prior to irradiation). Supernatant was analyzed by mutliplex bead-based flow cytometry. Only analytes detected above lower limit of quantification are displayed. Mean of two independent experiments, each run in duplicate, displayed.

Ccl5, *Il1r2* (IL1 receptor 2), *Il2rb*, *Il2ra*, *Ccr2*, *Ccr7*, and *Cxcl9*. In addition, we performed mRNA analysis on tumor cell populations sorted for CD45, which confirmed the large increases seen in *Ccl2*, *Ccl5*, and *Cxcl10* were predominantly from nonimmune cells (Fig. 5B). These data were compared with protein expression by cytokine array (Fig. 5C). Clear correlation between increased transcript levels and increased protein expression was observed for CCL2, CCL5, and CXCL10 in response to ATRi-RT. No differences were seen at this time point in IFN mRNA transcripts (data not shown).

Many proteins can bind dsDNA triggering an immune response, forming an innate immune recognition system for

dsDNA viruses. There has been significant recent interest in the ability of cGAS/STING to trigger inflammation through recognition of cytoplasmic host dsDNA (8, 18). We checked mRNA transcript results for TLRs or potential intracellular dsDNA-binding proteins, which may share functional similarity to STING, as well as cGAS, and STING/*Tmem173* themselves.

We observed an increase in cGAS by Western blot analysis in tumors treated with ATRi-RT, as well as an increase in the IFN-stimulated gene product IFIH1 (MDA-5; Fig. 5D). Analysis of gene expression data in the TC-1 tumors found statistically significant increases at the transcript level were present for *Tlr1*,*6*,*7*,*8*, and *Tlr9*, with the largest change in *Tlr9* (Fig. 5E). In keeping with a role for pattern recognition receptors, we also observed an increase in *Irf7* and *8* with combination therapy (Fig. 5F). increases in pattern recognition receptors for cytoplasmic nucleic acids (19): *Ddx58*/RIG-I and *Ifih1*/MDA5, both RNA sensors, and *Zbp1*/DAI (20) and *Ddx60* (21), which sense DNA. There was no change in STING (*Tmem173*) expression (Fig. 5G). When we performed the analysis on separated immune and tumor cells, we found that treatment induced significant increases in transcript levels in the nonimmune cells within the tumor (Fig. 5H). In all cases, as was observed for *in vitro* cytokine release, ATRi-RT led to the highest increase in transcript levels.

CCL2, CCL5, CXCL10, and CXCL9 increases indicate that ATRi, RT, and combination treatments induce proinflammatory responses. There was disparity between the clear significance observed at the transcript level versus protein expression. This was attributed to the 5-day posttreatment time point originally selected for gene expression analysis to favor assessment of infiltrating immune populations. In addition, both transcript and protein assessment were not tumor-specific. To bring clarity on both these points, cytokine release from 2 human head and neck squamous cell carcinoma cell lines *in vitro* was measured in response to ATRi, radiation, or in combination at 72 hours posttreatment (Fig. 5I and J). We observed maximal increase in CXCL10 and CCL3 secretion with the combination treatment (Fig. 5I and J), CCL5 increased, but there was no significant detection of CCL2. This suggests that part of the immune infiltration could be driven by tumor cell–intrinsic cytokine production. Almost without exception, radiation-induced cytokine and chemokine secretion from tumor cells was potentiated by the addition of ATRi.

Discussion

Radiotherapy is a standard-of-care in many tumor types. It is now well understood that radiotherapy can trigger immune responses and potentially lead to antitumor immunity (1). Despite advances in targeted delivery of radiotherapy, normal tissue toxicity imposes a limit upon further dose escalation. Small-molecule radiosensitizers such as ATRi present a potential means to improve responses to radiotherapy by increasing tumor-selective cell kill. Through broad profiling of the immune landscape, we have demonstrated preclinical evidence that combination therapy with ATR inhibition can modulate the radiation-induced inflammatory tumor microenvironment.

It has been recognized for some time that radiation has various effects on the tumor microenvironment, in particular, the infiltrating immune compartment. These effects can have positive and negative implications for tumor control (1). Radiation is also known to enhance the infiltration of immunosuppressive cells, such as $T_{regs,}$ TAMs, and MDSCs. These cells may increase the resistance of tumors to therapy and confer promalignant properties (4). Available preclinical data suggest there is no increased normal tissue toxicity from the combination of ATRi-RT (22, 23), but little is known about the effect of radiation-sensitizing drugs on the tumor microenvironment. It is increasingly recognized that targeted therapies may have immunomodulatory effects. For example, CDK4/6 inhibition has been shown to promote antitumor immunity, by increasing levels of intracellular double-stranded RNA, stimulating IFN production and antigen presentation, as well as by inhibiting T_{reg} proliferation (24). Treatment of tumor cell lines with PARP inhibitors causes upregulation of PD-L1, through a mechanism involving inactivation of GSK3α/β (25). It is also recognized that modulation of antitumor immunity may enhance radiation responses by overcoming the radiation-induced upregulation of immunosuppressive factors. For example, blocking the PD-L1 receptor overcomes radiation resistance, in a CD8-dependent manner (26). The picture that we have observed in this preclinical model is that ATRi in combination with radiation enhances infiltration of almost all immune populations. This appears to be a nonselective amplification of radiation-induced effects. As such, this results in increased infiltration of therapeutically beneficial cells such as DCs and $CD8^+$ CTLs, but also enhancement of potentially suppressive populations.

During this study, work by Vendetti and colleagues (27) demonstrated potentiation of radiation-induced cytotoxic T-cell activity when ATRi was added to 2×2 Gy radiation, as well as a reversal of the radiation-induced PD-L1 expression on tumor cells, a reduction in tumor-infiltrating $T_{regs,}$ and enhanced antitumor immunologic memory in a mouse model of colorectal cancer. Although no comment was made in that work about myeloid populations, the modulation of immune responses by ATRi-RT is notable, and highlights the differences in immune infiltrates and responses to therapy between tumor models, reflecting those seen in patients. This may be due to the differences in immunogenicity of the tumor model used, as well as differences in the capacity to respond to intracytoplasmic nucleic acids, and the spectrum of cytokines released by the tumor cells in response to DNA damage. We also note that the time point chosen for analysis may result in significant differences in the observed immune infiltrate, as noted by that work.

Functional assays are required to determine whether the $cd11b^+$ $Gr1^+$ cells are a truly immunosuppressive cell population, such as MDSCs. MDSCs suppress T-cell functions through depletion of arginine by arginases 1 and 2, and signaling to T cells, which results in dysfunction, proliferative arrest, and induction of the T_{reg} phenotype (28). Monocytic MDSCs can differentiate into TAMs and inflammatory DCs (29). The functions of Macs may be immunostimulatory (M1-like) or immunosuppressive (M2-like), depending upon their subtype (30). We have described ATRi amplification of radiation effects as indiscriminate, and this appears to extend to the vast majority of populations investigated. On preliminary analysis, there was no shift in Mac polarity based on the M2 marker CD206, but further analyses would be required to determine the properties of the infiltrating Macs. Immunosuppressive DCs have also been described in tumors, expressing indoleamine 2, 3-dioxygenase 1 (IDO-1) that suppresses T-cell activity (31). No significant changes in *Ido1* gene expression were observed in this experiment (but this was not verified on protein level; data not shown). Little change in subtype proportion was observed for Ly6C and Ly6G subpopulations with $CD11b^+$ $Gr\text{-}1^+$ cells.

We were interested in trying to identify the root cause behind the ability of ATRi to enhance radiation-induced immune cell infiltration. Interactions between the DDR and antitumor immunity are becoming better understood (6). We have previously shown that the mechanism of radiosensitization by AZD6738 involves mitotic catastrophe with the generation of acentric micronuclei (32). Recent data have shown these micronuclei are subject to breakdown of the micronuclear envelope that results in activation of cyclic GMP-AMP synthase (cGAS), which generates cyclic GMP-AMP (cGAMP), activating a type I IFN response via the STING pathway (18). Mitotic progression in the presence of micronuclei is required for their stimulation of immune responses (8). A previous study indicated that DDR-deficient breast tumors were defined by IFN signaling (7). In that study, CXCL10 and CCL5 were significantly upregulated in DNA repair–deficient cells in a cGAS/STING–dependent manner with chemoattraction of PBMCs dependent on CXCL10 and CCL5. The similarity of radiation and ATRi (a pharmacologically induced DDR defect) with regard to CXCL10 and CCL5 expression was striking.

These recent findings in the literature lead us to look at transcriptional levels of STING where no increase was observed. This does not preclude STING functional activity at a steady gene expression state. Levels of cGAS and transcriptional levels of a number of other potential nucleic acid–sensing proteins were, however, upregulated coinciding with increased *Irf7*. There was a significant increase in Z-DNA–binding protein 1 (*Zbp1*), in ATRi-RT versus control. ZBP1 is a cytosolic DNA sensor, which stimulates type-I IFN production and the production of CXCL10 signaling through IRF3 and IRF7 (20). Cytosolic DNA can also activate RIG-I (*Ddx58*) via DNA-dependent RNA polymerase III signaling (33). RIG-I stimulation has been shown to cause CXCL10 and CCL5 release from tumor cells and upregulate HLA class I (34). Another RNA sensor, IFN-induced helicase C domain–containing protein-1 (*Ifih1*) also causes CXCL10 release upon stimulation (35). *Rsad2*/viperin was increased under all treatments and is an IFN-inducible gene promoting TLR9 signaling in pDC (15). This pathway detects viral and self-DNA, stimulating the transcription of type I IFN by signaling through IRF7. We recognize that other pathways may also be involved in the inflammatory response to radiation, including absent in melanoma 2 (AIM2; ref. 36), whether these are modulated by the addition of ATRi is currently not known.

Because of the 5-day postradiation time point, only indirect evidence of a type-I IFN response after ATRi-RT treatment was shown by the upregulation of multiple IFN-stimulated genes (ISG) in tumor cells (37). The outlined nucleic acid sensors are known to be ISGs. Hence, we cannot definitively state whether these genes are induced in response to cytosolic nucleic acids directly, or in response to type-I IFN production from a different source. It is unlikely that elevated levels of these proteins are not functionally active in some capacity in sensing cytoplasmic dsDNA in response to radiation and ATRi. Future work is needed to establish the exact functional relevance of these proteins.

In vitro cell line experiments and gene expression analysis of sorted immune and nonimmune cells, showed cytokines produced by proliferating tumor cells subjected to radiation and ATRi are likely to contribute significantly to the immune infiltration observed. In our model, tumor cells alone secreted CXCL10 and CCL5 with combination treatment. CCL5 is chemotactic for Macs and T cells, and plays a role in activating NK cells (in conjunction with signals from activated T cells). Hence, DNA damage may activate DNA-sensing pathways within the cell to cause release of CXCL10 and CCL5, attracting innate immune cells into the tumor, which subsequently activate an adaptive response. CCL5 (i) is a target of NF-κB activity, again released by multiple cell types including immune, stromal, and tumor cells, (ii) recruits cells including T cells and Macs, and (iii) stimulates NK-cell activation. CCL5, along with CCL2, has also been implicated in cancer progression and metastasis, through multiple mechanisms, including the generation of MDSCs (38–40), and the attraction of inflammatory monocytes, which subsequently differentiate into Macs capable of promoting metastasis (41, 42). CCL2 is secreted by multiple cell types, including tumor cells and endothelial cells, with the major source being monocytes/Macs (43) Tumor-associated Macs also produce CCL22 that attracts T_{regs} (31). *Ccl22* is one of the significantly upregulated genes with the ATRi-RT combination versus control (Fig. 5A and B). Overall, our data support the hypothesis that DNA damage within the tumor cells leads to an IFN response, and cytokine release leading to modulation of the immune microenvironment. The addition of ATRi boosts this radiation-induced response.

Publications in the literature have shown positive preclinical results for radiation in combination with anti-PD1 (44) and anti-CTLA4 (45) therapies. Our data point to a myeloid-heavy infiltrate in response to ATRi-RT. This may offer an alternative immuno-oncology angle of attack where anti-PD1 or -CTLA4 fails. Translational research from the ongoing AZD6738 and radiation clinical trial may also give further information about the immunogenicity of the combination. We have chosen to investigate the effects of ATRi on a clinically relevant radiation dose schedule of 2 Gy per fraction, most commonly used in radical treatments, and the dose per fraction currently being assessed in the clinical study of AZD6738 with radiation (46). We acknowledge that optimal dose-fractionations for immune stimulation are still under investigation, and are likely to be moderately large doses per fraction. The effect of radiosensitizers on these dose-fractionations is the subject of ongoing study, but in the clinic, drug sensitization of large fractions is avoided due to concerns regarding toxicity. In the radiation field, analysis of fractionation effects with radiosensitizing drugs to see whether they can be optimized not only for tumor kill, but potentially selection of a more favorable profile of immune infiltrates would be of great interest.

In conclusion, we have shown an immunomodulatory effect of ATR inhibition with radiotherapy on the tumor microenvironment. Radiosensitization by ATRi is well established, but to fully exploit the potential of G_2–M cell-cycle checkpoint-targeted agents in cancer treatment, we need to understand the effect of these agents on immune responses. ATR inhibition can boost the immunogenic response to radiotherapy. Understanding the suppressive immune populations in this context is critical to enhancing antitumor immunity in addition to the enhanced tumor control possible through the combination of ATRi and radiation.

Disclosure of Potential Conflicts of Interest

A. Sadanandam reports receiving commercial research grants from Merck KGaA; reports receiving other commercial research support from Pierre Fabre; and is listed as an inventor on a patent involving colorectal cancer classification with different prognosis and therapeutic responses, a patent involving prognostic and treatment response prediction in gastric cancer, and a patent involving patient classification and prognostic method. K. J. Harrington reports

receiving commercial research grants from AstraZeneca and MSD; reports receiving speakers bureau honoraria from AstraZeneca, MSD, Merck-Serono, and Bristol-Myers Squibb; and is a consultant/advisory board member for AstraZeneca, MSD, Merck-Serono, Bristol-Myers Squibb, and Pfizer. No potential conflicts of interest were disclosed by the other authors.

Authors' Contributions

Conception and design: M.T. Dillon, M. McLaughlin, K.J. Harrington
Development of methodology: M.T. Dillon, K.F. Bergerhoff, M. McLaughlin, K.J. Harrington
Acquisition of data (provided animals, acquired and managed patients, provided facilities, etc.): M.T. Dillon, K.F. Bergerhoff, M. Pedersen, E.C. Patin, H. Whittock, E. Crespo-Rodriguez, A. Pearson, J.T. Paget, H.G. Smith, S. Foo, G. Bozhanova, C. Ragulan, E. Fontana, K. Desai, A.C. Wilkins, M. McLaughlin
Analysis and interpretation of data (e.g., statistical analysis, biostatistics, computational analysis): M.T. Dillon, E.C. Patin, J.T. Paget, M. McLaughlin, K.J. Harrington
Writing, review, and/or revision of the manuscript: M.T. Dillon, M. Pedersen, E.C. Patin, E. Crespo-Rodriguez, H.G. Smith, E. Fontana, K. Desai, A.C. Wilkins, A. Melcher, M. McLaughlin, K.J. Harrington
Administrative, technical, or material support (i.e., reporting or organizing data, constructing databases): M.T. Dillon, R.R. Patel
Study supervision: M.T. Dillon, A. Sadanandam, M. McLaughlin, K.J. Harrington

Acknowledgments

The authors would like to thank AstraZeneca for supplying AZD6738. This study was supported by Cancer Research United Kingdom (grant no. C7224/A13407), RM/ICR NIHR Biomedical Research Centre, Rosetrees Trust (grant nos. M48 and M444, to M.T. Dillon and K.J. Harrington), and Anthony Long Charitable Trust (to K.J. Harrington). M.T. Dillon is a Cancer Research United Kingdom Clinical Research Fellow. The Institute of Cancer Research and Royal Marsden have received funding for a phase I study of AZD6738, which is partially funded by AstraZeneca.

The costs of publication of this article were defrayed in part by the payment of page charges. This article must therefore be hereby marked *advertisement* in accordance with 18 U.S.C. Section 1734 solely to indicate this fact.

Received June 28, 2018; revised December 9, 2018; accepted February 11, 2019; published first February 15, 2019.

References

1. Weichselbaum RR, Liang H, Deng L, Fu YX. Radiotherapy and immunotherapy: a beneficial liaison? Nat Rev Clin Oncol 2017;14:365–79.
2. Barker HE, Paget JT, Khan AA, Harrington KJ. The tumour microenvironment after radiotherapy: mechanisms of resistance and recurrence. Nat Rev Cancer 2015;15:409–25.
3. Demaria S, Golden EB, Formenti SC. Role of local radiation therapy in cancer immunotherapy. JAMA Oncol 2015;1:1325–32.
4. Vatner RE, Formenti SC. Myeloid-derived cells in tumors: effects of radiation. Semin Radiat Oncol 2015;25:18–27.
5. Barber GN. STING: infection, inflammation and cancer. Nat Rev Immunol 2015;15:760–70.
6. Mouw KW, Goldberg MS, Konstantinopoulos PA, D'Andrea AD. DNA damage and repair biomarkers of immunotherapy response. Cancer Discov 2017;7:675–93.
7. Parkes EE, Walker SM, Taggart LE, McCabe N, Knight LA, Wilkinson R, et al. Activation of STING-dependent innate immune signaling by S-phase-specific DNA damage in breast cancer. J Natl Cancer Inst 2017;109:djw199.
8. Harding SM, Benci JL, Irianto J, Discher DE, Minn AJ, Greenberg RA. Mitotic progression following DNA damage enables pattern recognition within micronuclei. Nature 2017;548:466–70.
9. Vanneman M, Dranoff G. Combining immunotherapy and targeted therapies in cancer treatment. Nat Rev Cancer 2012;12:237–51.
10. Workman P, Aboagye EO, Balkwill F, Balmain A, Bruder G, Chaplin DJ, et al. Guidelines for the welfare and use of animals in cancer research. Br J Cancer 2010;102:1555–77.
11. Lin KY, Guarnieri FG, Staveley-O'Carroll KF, Levitsky HI, August JT, Pardoll DM, et al. Treatment of established tumors with a novel vaccine that enhances major histocompatibility class II presentation of tumor antigen. Cancer Res 1996;56:21–6.
12. Dillon MT, Espinasse A, Ellis S, Mohammed K, Grove LG, McLellan L, et al. Abstract CT084: A Phase I dose-escalation study of ATR inhibitor monotherapy with AZD6738 in advanced solid tumors (PATRIOT Part A). Cancer Res 2017;77:CT084.
13. Samarajiwa SA, Forster S, Auchettl K, Hertzog PJ. INTERFEROME: the database of interferon regulated genes. Nucleic Acids Res 2009;37:D852–D7.
14. Marvel D, Gabrilovich DI. Myeloid-derived suppressor cells in the tumor microenvironment: expect the unexpected. J Clin Invest 2015;125:3356–64.
15. Swiecki M, Colonna M. The multifaceted biology of plasmacytoid dendritic cells. Nat Rev Immunol 2015;15:471–85.
16. Kuang DM, Zhao Q, Peng C, Xu J, Zhang JP, Wu C, et al. Activated monocytes in peritumoral stroma of hepatocellular carcinoma foster immune privilege and disease progression through PD-L1. J Exp Med 2009;206:1327–37.
17. Lu C, Redd PS, Lee JR, Savage N, Liu K. The expression profiles and regulation of PD-L1 in tumor-induced myeloid-derived suppressor cells. Oncoimmunology 2016;5:e1247135.
18. Mackenzie KJ, Carroll P, Martin CA, Murina O, Fluteau A, Simpson DJ, et al. cGAS surveillance of micronuclei links genome instability to innate immunity. Nature 2017;548:461–5.
19. Paludan SR, Bowie AG. Immune sensing of DNA. Immunity 2013;38:870–80.
20. Takaoka A, Wang Z, Choi MK, Yanai H, Negishi H, Ban T, et al. DAI (DLM-1/ZBP1) is a cytosolic DNA sensor and an activator of innate immune response. Nature 2007;448:501–5.
21. Miyashita M, Oshiumi H, Matsumoto M, Seya T. DDX60, a DEXD/H box helicase, is a novel antiviral factor promoting RIG-I-like receptor-mediated signaling. Mol Cell Biol 2011;31:3802–19.
22. Dunne V, Ghita M, Small DM, Coffey CBM, Weldon S, Taggart CC, et al. Inhibition of ataxia telangiectasia related-3 (ATR) improves therapeutic index in preclinical models of non-small cell lung cancer (NSCLC) radiotherapy. Radiother Oncol 2017;124:475–81.
23. Vendetti FP, Leibowitz BJ, Barnes J, Schamus S, Kiesel BF, Abberbock S, et al. Pharmacologic ATM but not ATR kinase inhibition abrogates p21-dependent G1 arrest and promotes gastrointestinal syndrome after total body irradiation. Sci Rep 2017;7:41892.
24. Goel S, DeCristo MJ, Watt AC, BrinJones H, Sceneay J, Li BB, et al. CDK4/6 inhibition triggers anti-tumour immunity. Nature 2017;548:471–5.
25. Jiao S, Xia W, Yamaguchi H, Wei Y, Chen MK, Hsu JM, et al. PARP Inhibitor upregulates PD-L1 expression and enhances cancer-associated immunosuppression. Clin Cancer Res 2017;23:3711–20.
26. Dovedi SJ, Adlard AL, Lipowska-Bhalla G, McKenna C, Jones S, Cheadle EJ, et al. Acquired resistance to fractionated radiotherapy can be overcome by concurrent PD-L1 blockade. Cancer Res 2014;74:5458–68.
27. Vendetti FP, Karukonda P, Clump DA, Teo T, Lalonde R, Nugent K, et al. ATR kinase inhibitor AZD6738 potentiates CD8+ T cell-dependent antitumor activity following radiation. J Clin Invest 2018;128:3926–40.
28. Marigo I, Dolcetti L, Serafini P, Zanovello P, Bronte V. Tumor-induced tolerance and immune suppression by myeloid derived suppressor cells. Immunol Rev 2008;222:162–79.
29. Veglia F, Perego M, Gabrilovich D. Myeloid-derived suppressor cells coming of age. Nat Immunol 2018;19:108–19.
30. Szebeni GJ, Vizler C, Nagy LI, Kitajka K, Puskas LG. Pro-tumoral inflammatory myeloid cells as emerging therapeutic targets. Int J Mol Sci 2016;17:1958.
31. Gabrilovich DI, Ostrand-Rosenberg S, Bronte V. Coordinated regulation of myeloid cells by tumours. Nat Rev Immunol 2012;12:253–68.

32. Dillon MT, Barker HE, Pedersen M, Hafsi H, Bhide SA, Newbold KL, et al. Radiosensitization by the ATR inhibitor AZD6738 through generation of acentric micronuclei. Mol Cancer Ther 2017;16:25–34.
33. Chiu YH, MacMillan JB, Chen ZJ. RNA polymerase III detects cytosolic DNA and induces type I interferons through the RIG-I pathway. Cell 2009; 138:576–91.
34. Kubler K, Gehrke N, Riemann S, Bohnert V, Zillinger T, Hartmann E, et al. Targeted activation of RNA helicase retinoic acid-inducible gene-I induces proimmunogenic apoptosis of human ovarian cancer cells. Cancer Res 2010;70:5293–304.
35. Glas M, Coch C, Trageser D, Dassler J, Simon M, Koch P, et al. Targeting the cytosolic innate immune receptors RIG-I and MDA5 effectively counteracts cancer cell heterogeneity in glioblastoma. Stem Cells 2013;31:1064–74.
36. Hu B, Jin C, Li HB, Tong J, Ouyang X, Cetinbas NM, et al. The DNA-sensing AIM2 inflammasome controls radiation-induced cell death and tissue injury. Science 2016;354:765–8.
37. Schneider WM, Chevillotte MD, Rice CM. Interferon-stimulated genes: a complex web of host defenses. Annu Rev Immunol 2014;32:513–45.
38. Aldinucci D, Colombatti A. The inflammatory chemokine CCL5 and cancer progression. Mediators Inflamm 2014;2014:292376.
39. Zhang Y, Lv D, Kim HJ, Kurt RA, Bu W, Li Y, et al. A novel role of hematopoietic CCL5 in promoting triple-negative mammary tumor progression by regulating generation of myeloid-derived suppressor cells. Cell Res 2013;23:394–408.
40. Kumar V, Patel S, Tcyganov E, Gabrilovich DI. The nature of myeloid-derived suppressor cells in the tumor microenvironment. Trends Immunol 2016;37:208–20.
41. Qian BZ, Li J, Zhang H, Kitamura T, Zhang J, Campion LR, et al. CCL2 recruits inflammatory monocytes to facilitate breast tumor metastasis. Nature 2011;475:222–5.
42. Lim SY, Yuzhalin AE, Gordon-Weeks AN, Muschel RJ. Targeting the CCL2-CCR2 signaling axis in cancer metastasis. Oncotarget 2016;7:28697–710.
43. Deshmane SL, Kremlev S, Amini S, Sawaya BE. Monocyte chemoattractant protein-1 (MCP-1): an overview. J Interferon Cytokine Res 2009;29:313–26.
44. Oweida A, Lennon S, Calame D, Korpela S, Bhatia S, Sharma J, et al. Ionizing radiation sensitizes tumors to PD-L1 immune checkpoint blockade in orthotopic murine head and neck squamous cell carcinoma. Oncoimmunology 2017;6:e1356153.
45. Dewan MZ, Galloway AE, Kawashima N, Dewyngaert JK, Babb JS, Formenti SC, et al. Fractionated but not single-dose radiotherapy induces an immune-mediated abscopal effect when combined with anti-CTLA-4 antibody. Clin Cancer Res 2009;15:5379–88.
46. Dillon MT, Boylan Z, Smith D, Guevara J, Mohammed K, Peckitt C, et al. PATRIOT: a phase I study to assess the tolerability, safety and biological effects of a specific ataxia telangiectasia and Rad3-related (ATR) inhibitor (AZD6738) as a single agent and in combination with palliative radiation therapy in patients with solid tumours. Clin Transl Radiat Oncol 2018;12: 16–20.